Detailed Methods

Animal models. Wild-type mice on an FVB or C57BL/6 background, OCT1/2 double knockout (OCT1/2$^{-/-}$; 006622), athymic male nude mice (CrTac:NCr-Fox1^{nu}; NCRNU-M), and wild-type cannulated (carotid artery; CAC-R) Sprague dawley rats were purchased from Taconic Biosciences. OCT2$^{-/-;tm1sage}$ Sprague dawley rats, containing a biallelic deletion within the *Slc22a2* gene were purchased from Horizon Discovery (strain code: TGRS6580), currently ENVIGO. This animal model and its preliminary characterization is presented in **Supplemental Figure 4A-C**. OATP2B1-deficient (OATP2B1$^{-/-}$) mice were generated from KOMP repository embryos (Slco2b1^{tm1a}, Design ID: 42989) and re-derived at the GEMM core facility at The Ohio State University, with the assistance of Dr. Vincenzo Coppola. OATP2B1-deficient mice were generated by targeted exon 4 deletion through Flp-Frt and Cre-loxP recombination, resulting in decreased absorption and increased bioavailability of orally administered substrates, such as fluvastatin (1). Dr. Joanne Wang (University of Washington, Seattle, Washington, USA) provided the OCT3-deficient mice, which were generated by targeted disruption of the gene promotor and exon 1. OCT3-deficient mice display diminished accumulation of OCT3 substrates, such as MPP into the heart and embryos due to altered placenta-mediated maternal to fetal transport (2). Dr. Yukio Kato (Kanazawa University, Kanazawa, Japan) provided the OCTN1-deficient mice, which were generated by targeted disruption of exon 1 resulting in the deletion of the start codon and transcription of OCTN1 mRNA. OCNT1-deficient mice display diminished absorption of OCTN1-specific substrate, ergothioneine (ETT), and accumulation of ETT into OCTN1-expressing tissues such as the intestine, liver, and kidneys (3). Dr. Yan Shu (University of Maryland, Baltimore, Maryland, USA) provided the MATE1-deficient mice, which were generated using a gene trap vector approach targeting the region of intron 10. The loss of MATE1 display diminished accumulation of metformin in the liver and kidneys, and increased systemic exposure of cationic-type substrate such as paraquat. The deletion of MATE1 has been associated with increased deterioration of the kidneys through excessive accumulation of toxic xenobiotics (4) . Drs. Richard

B. Kim (Western University, London, Ontario, Canada) and Jeffrey L. Stock (Pfizer, Groton, Connecticut, USA) provided the OATP1B2-deficient mice, which were generated by targeted excision of exon 10 to 12 and results in significantly altered disposition of prototypical OATP1B-type substrates, such as pravastatin and rifampin (5). All animals were housed in a temperature-controlled environment with a 12-hour light cycle, given standard chow diet and water ad libitum, and handled according to the Animal Care and Use Committee of The Ohio State University, under an approved protocol (2015A00000101-R1). All animals were maintained through in-house breeding with the exception of wild-type FVB mice, athymic nude mice, and Sprague dawley rats.

Cellular accumulation. Uptake experiments were performed using radio-labeled oxaliplatin and various prototypical substrates for the examined transporters of interest, including tetraethylammonium, ergothioneine, estradiol-β-glucuronide, and fluvastatin in the presence or absence of the known transport inhibitors: dasatinib (for cells expressing OCT1, OCT2, OCT3, or MATE1), 6-[(4-Nitrobenzyl)thio]-9-β-D-ribofuranosylpurine (NBMPR; for cells expressing OCTN1), and nilotinib (for cells expressing OATP1B1, OATP1B2, OATP1B3, or OATP2B1). The cDNA for the mouse, rat, or human plasmids were obtained from Origene, and the reconstructed cDNA was subcloned into an empty vector, transfected into HEK293 cells, followed by selection with geneticin (G418) or hygromycin. The cells are kept in the presence of the selection agent during passage and maintenance. Prior to uptake experiments, cells were grown to 90% confluence on poly-lysine coated multi-well plates. For uptake, cells were briefly rinsed with warm 1X PBS and incubated in the presence or absence of a vehicle or inhibitor, prepared in serum and phenol-red free DMEM for 15 minutes (pre-treatment). The pre-treatment was rinsed off with warm 1X PBS followed by the addition of radiolabeled compounds for 5 – 30 minutes. After incubation, transport was halted by aspirating radiolabeled drug, and rinsing the cells with ice-cold 1X PBS three times. Total radioactivity originating from the substrates was measured by lysing the cells with 1N NaOH, neutralized with 2N HCL, and measuring intracellular radioactivity,

by liquid scintillation counting and normalizing to total protein levels. he validity of these overexpressed models to transport prototypical substrates is documented in **Supplemental Table 1**.

Peripheral neurotoxicity assessment.

Experimental models of oxaliplatin-induced peripheral neurotoxicity (OIPN) have been previously described (6, 7). Preliminary studies indicated that the degree and time-course of OIPN phenotypes in mice were independent of sex and background strain (**Supplemental Figure 1 B-C**). For acute assessment, animals received a single intra-peritoneal injection of oxaliplatin (dose, 10 mg/kg) dissolved in a 5% glucose solution, or vehicle. Oxaliplatin-induced mechanical allodynia was measured using the Von Frey Hairs test, measuring the force (in g) required to elicit paw withdrawal before and at 24 h after oxaliplatin administration, expressed as a percentage change from baseline. All animals were allowed to acclimate enclosed atop a wire mesh for 60 min prior to sensitivity testing. For studies evaluating chronic neurotoxicity, oxaliplatin (dose, 4 mg/kg) was administered twice a week by intra-peritoneal injection for four weeks (cumulative dose 32 mg/kg).

A clinical electro-diagnostic system (Ultra Pro S100, Natus Neurology) was used to perform nerve conduction studies. The supramaximal action potential amplitude (AMP) and the nerve conduction velocity (NCV) were measured for the caudal and digital nerve, 48 hours before treatment (baseline), during treatment (2 weeks), and at the end of the experiment. Stimulating electrodes were placed on the fourth digit of the hind paw, and two recording electrodes were placed 10 mm proximally, near the ankle. Similarly, stimulating electrodes were placed at the base of the tail, and two recording electrodes were placed 35 mm proximally, on the tail. For both the digital and caudal nerve, a total of 10 supramaximal stimulations were delivered. Velocity was calculated as a ratio of the distance from stimulating electrodes divided by the distant latency, and amplitude from peak-to-peak. Mice were maintained under isoflurane anesthesia delivered

via nosecone and the body temperature was controlled during the recordings with a heating pad. AMP and NCV were normalized and expressed as a percent change from baseline, due to inter-experimental variability in baseline recordings.

DRG isolation and satellite glial cell culture. DRGs were extracted from male or female animals [thoracic position 8 (T8) to lumbar position 5 (L5)]. Culturing of primary satellite cells from extracted DRGs was performed according to a previously published procedure (8). Briefly, DRGs from animals were collected in PBS without Ca^{2+} and Mg^{2+}, supplemented with antibiotics and D-glucose. The DRGs were digested in type II collagenase for 60 min at 37 ℃ followed by additional digestion with 0.25% trypsin for 10 min. The trypsin was neutralized by the addition of DMEM containing 10% FBS and 1% penicillin/streptomycin. Subsequent mechanical disassociation by pipetting was used to release satellite cells. The digested DRGs were transferred to a 25-cm^2 flask and incubated for an additional 2-3 hours. Satellite cells remain attached to the flask while neurons and neuronal debris from the DRGs remain in suspension. DRGs were also collected in RNALater or snap frozen for RNA and/or determination of total platinum, respectively.

Gene Expression Analysis. RNA from mouse or rat DRGs, or primary cultured satellite cells was extracted using an Omega Extraction kit, according to manufacturer's protocol. Samples were analyzed using real-time quantitative PCR and Taqman Probes (Applied Biosystems) or the Mouse Transporter RT^2 PCR custom array system containing ABC and SLC transporter genes or Human Transporter RT^2 Profiles PCR (SABiosciences). Briefly, RNA from DRG (thoracic position 8 to lumbar position 5) were extracted from wild-type or transporter-deficient mice or rats. The relative gene expression was determined using the $\Delta\Delta$Ct method, and normalized to the mouse, rat or human housekeeping gene, *GAPDH*.

Immunohistochemistry. L4 and L5 DRG were collected from mice or rats and incubated overnight in 4% para-formaldehyde at room temperature, followed by PBS washing. DRGs were incubated overnight at 4℃ in 20% sucrose, embedded in OCT, and snap frozen on dry ice. After cryo-sectioning, slides were brought back to room temperature and fixed for 15 min in 4% PFA. Permeabilization was performed using 1% Triton X-100 in PBS for 10 min, then blocked with 2% BSA in a buffer containing 0.1% Tween 20 for 1 hour. Primary antibody (rat OCT2.1-A, Alpha Diagnostic) was used at 1:300 at 4℃ and secondary antibody (Alexa Fluor 647 goat anti rabbit IgG; Invitrogen) at 1:300 for 1 h in the dark. Slides were mounted with ProLong Gold anti-fade reagent with DAPI (Life Technologies) and pictures were taken with a confocal microscope (Nikon A1R).

Pharmacokinetic Studies. To determine the plasma concentration-time profiles of oxaliplatin in mice, serial whole blood samples were collected from the submandibular vein for the initial three time-points, from the retro-orbital sinus vein for the subsequent two time-points, and cardiac puncture at the terminal time-point (9). Blood samples were centrifuged at 11,000 rpm for 5 min, and the plasma supernatants collected and stored at -80℃ until analysis. Carotid-artery catheterized Sprague dawley rats were used for blood sampling according to manufacturer recommendations, while metabolic cages were used to collect urine samples. Tissues were homogenized in 0.2% nitric acid with stainless steel beads. Concentrations of total platinum, as a surrogate marker for oxaliplatin levels, in plasma, urine, or homogenized tissues, were determined by flameless atomic absorption spectroscopy (PinAAcle900z; PerkinElmer) following pretreatment with 0.2% nitric acid.

Colorectal Xenograft. HEK293T cells were co-transfected with a lentiviral vector pCDH-EF1a-eFFly-eGFP (Addgene, 104834) and packaging plasmids psPAX and pMD2.G. The viruses were collected after 48 hours and infected into the colon cancer cells HCT116, and sorted for GFP

positivity. After expansion, $2x10^6$ million cells per 100 µL (re-suspended 10% FBS McCoy's 5A media) were subcutaneously injected into the left and right rear flanks of male athymic nude mice (Taconic). Mice were randomized into groups after reaching an average tumor size of 150 mm^3, determined by digital calipers following the formula: $V = W^2 \times L/2$. Mice received vehicle, oxaliplatin (dose, 4 mg/kg) or oxaliplatin plus dasatinib (dose, 4 mg/kg plus 15 mg/kg). The cumulative oxaliplatin dose of 32 mg/kg is similar to the dose received to elicit chronic mechanical allodynia. In these experiments, oxaliplatin was given as an intra-peritoneal injection while dasatinib was given orally, 30 min before oxaliplatin. Tumor volume was measured by digital calipers twice per twice or once per week by bioluminescence imaging (IVIS Lumina II).

Statistical Analysis. Data presented represent the mean ± SEM of repeat observation made before or after normalization to baseline values. All experiments were performed in multiple replicates, unless stated otherwise, and repeated on at least two occasions. An unpaired two-sided Student's t test with Welch's correction (2 groups) or a one-way ANOVA with Dunnett's post-hoc test (>2 groups) was used to evaluate statistical significance using $P<0.05$ as the cut-off.

Supplemental Table 1. Transport of probe substrates			
Transporter	**Species**	**Substrate**	**Fold-Change**
OCT1	Murine	TEA	10.5 ± 0.37
	Human	TEA	13.1 ± 1.27
OCT2	Murine	TEA	11.3 ± 1.77
	Rat	TEA	9.40 ± 1.36
	Human	TEA	9.30 ± 1.23
OCT3	Murine	TEA	14.9 ± 0.70
	Human	TEA	9.99 ± 0.11
OCTN1	Murine	ETT	14.2 ± 0.47
	Human	ETT	17.3 ± 1.79
OATP1B1	Human	EβG	4.61 ± 0.15
OATP1B3	Human	EβG	3.31 ± 0.92
OATP1B2	Murine	EβG	3.57 ± 1.88
OATP2B1	Murine	Fluvastatin	6.38 ± 1.73
	Human	Fluvastatin	3.66 ± 1.45
MATE1	Murine	TEA	9.81 ± 0.74
	Human	TEA	17.8 ± 1.23

Supplemental Table 1. Validation of mouse, rat, or human overexpression models by evaluating their ability to accumulate known prototypical transport substrates. Fold-change is expressed as the uptake kinetics (pmol/mg protein/min) of overexpressing cells divided by vector-transfected control cells. Abbreviations: TEA; tetraethylammonium, ETT; ergothioneine, or EβG; estradiol β glucuronide.

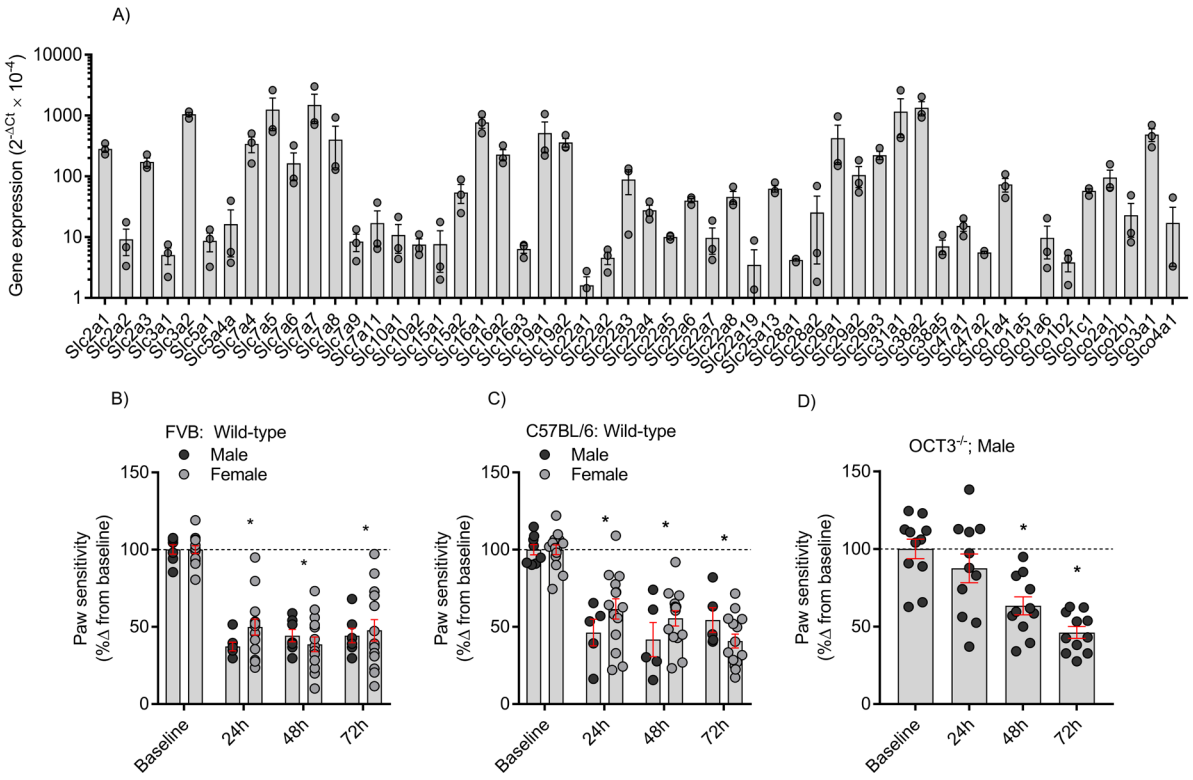

Supplemental Figure 1. (A) Gene expression profile of SLCs examined from the Mouse Transporter RT^2 PCR custom array (SABiosciences; 330231) from untreated, wild-type FVB DRGs. **(B-D)** Evaluation of oxaliplatin-induced mechanical allodynia in wild-type male or female FVB, C57BL/6, or male OCT3$^{-/-}$ up to 72 hours following treatment with a single injection of 10 mg/kg oxaliplatin (n= 6-12 per group). OCT1/2-, OCT3-, and MATE1-deficient mice are established on an FVB background. OCTN1- and OATP2B1-deficient mice are established on a C57BL/6 background. OATP1B2-deficient mice are established on a DBA/J backrground. Paw sensitivity presented represents the percentage change and mean ± standard error of the mean (SEM) from baseline values. *P<0.05 compared to baseline or wild-type values.

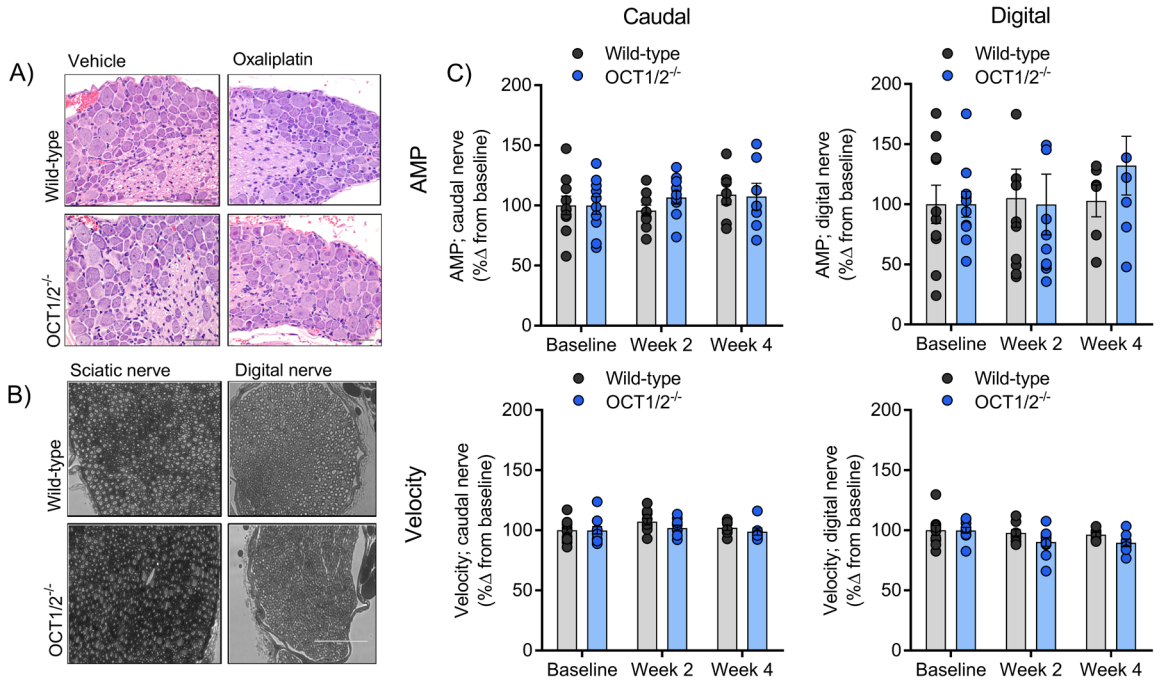

Supplemental Figure 2. (A) Cross sections of mouse DRGs stained with H&E, magnification 100x. **(B)** Morphometry of sciatic and caudal nerves in wild-type or OCT1/2$^{-/-}$ after multiple treatments with oxaliplatin, magnification 100x. **(C)** Nerve conduction studies (NCS) (maximal amplitude and velocity) of the digital and caudal nerve from OCT1/2$^{-/-}$ mice. All animals received multiple intraperitoneal injections of 4.0 mg/kg oxaliplatin twice per week for four weeks (cumulative dose 32 mg/kg). Data presented represents the percentage change and mean ± standard error of the mean (SEM) from baseline values.

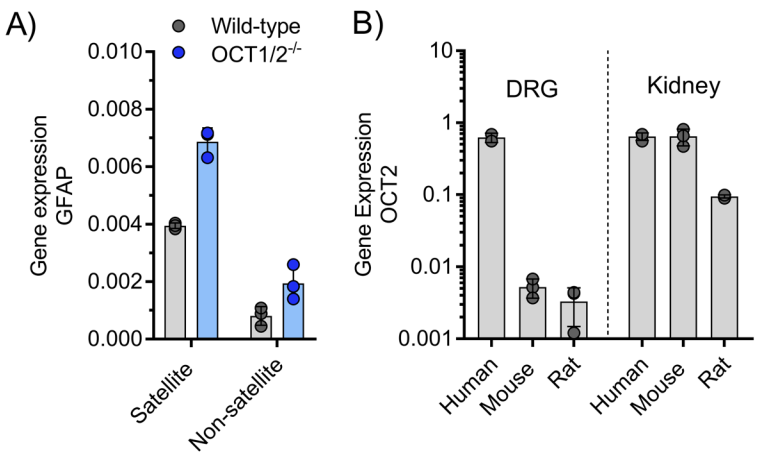

Supplemental Figure 3. (A) GFAP expression in satellite and non-satellite glial cells from untreated wild-type or OCT1/2$^{-/-}$ mice (n=4) to demonstrate isolation technique. **(B)** Comparative expression profile of human, mouse and rat kidneys and DRGs using the formula: 2^{-dCt} target minus GAPDH method.

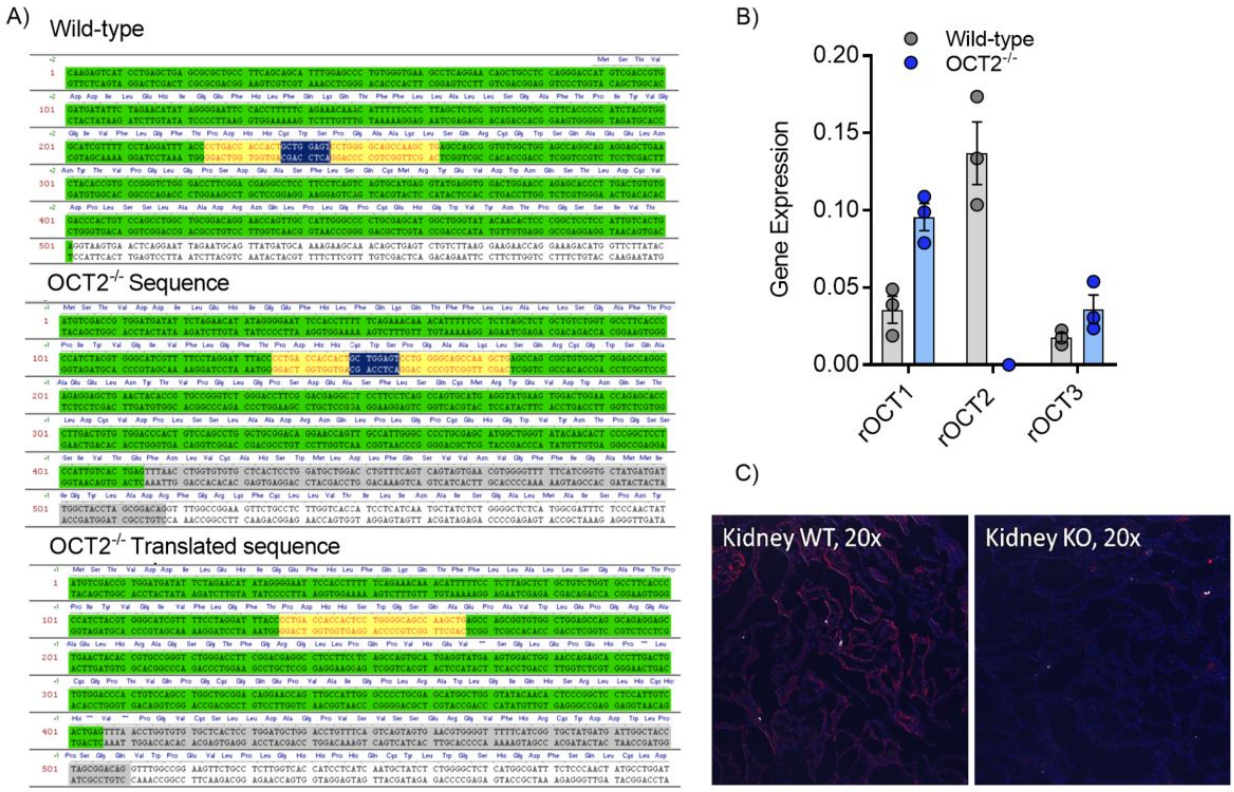

Supplemental Figure 4. (A) Sequencing of wild-type or OCT2$^{-/-}$ rat sequences provided by Horizon Discovery, now ENVIGO (strain code: TGRS6580). **(B)** Characterization of kidneys in OCT2$^{-/-}$ rats by RT-PCR and **(C)** immunofluorescence staining of kidney cross sections (red = rOCT2 and blue = DAPI), magnification 20x.

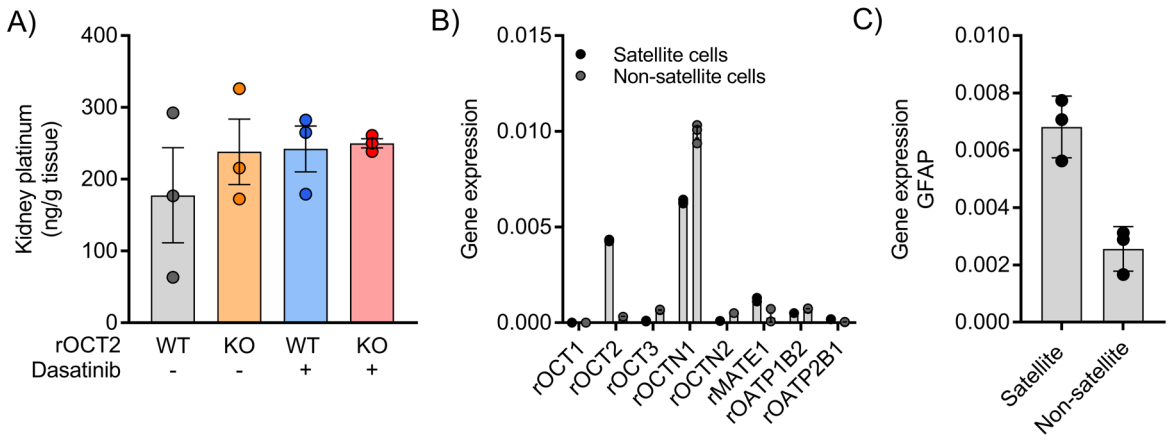

Supplemental Figure 5. (A) Platinum concentrations in kidneys isolated from wild-type or OCT2$^{-/-}$ rats treated with either oxaliplatin and citric acid or oxaliplatin (10 mg/kg) and dasatinib (15 mg/kg) (n=3). **(B)** Transporter expression in satellite and non-satellite cells isolated from DRGs in *ex vivo* primary cultures to demonstrate expression differences in phylogenetically-linked DRG transporters. **(C)** GFAP expression in wild-type rats to demonstrate isolation technique. Data presented represents the mean ± standard error of the mean (SEM).

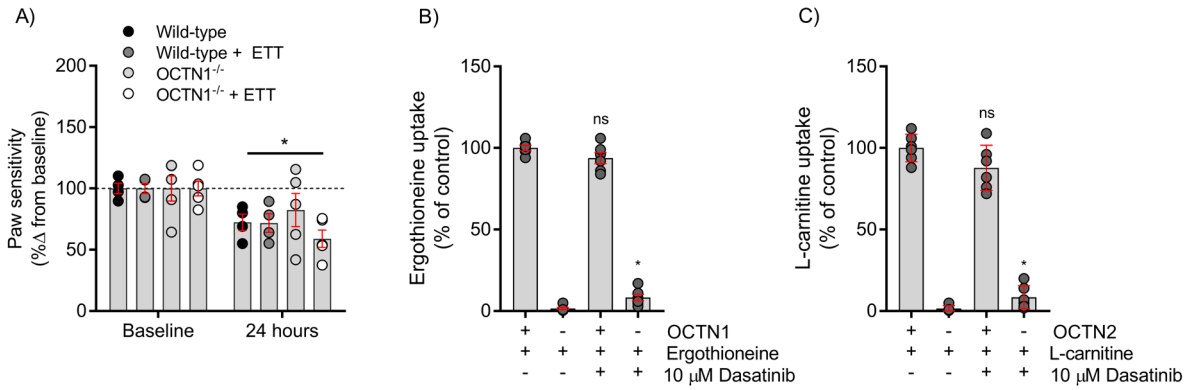

197

198 **Supplemental Figure 6. (A)** Oxaliplatin-induced mechanical allodynia in male wild-type or
199 OCTN1$^{-/-}$ mice 24 hours after following treatment with a single injection of 10 mg/kg oxaliplatin
200 (n= 4-6). Ergothioneine (30 mg/kg) or vehicle (0.9% saline) was administered intravenously 30
201 minutes prior oxaliplatin injections. Paw sensitivity presented represents the percentage change
202 and mean ± standard error of the mean (SEM) from baseline. **(B)** Inhibition of human OCTN1 or
203 **(C)** OCTN2 by pre-treatment with 10 μM dasatinib. Relative uptake is expressed as a percentage
204 change compared to control (uptake in OCTN1- or OCTN2-expressing cells). *P<0.05 compared
205 to baseline or control values.

206

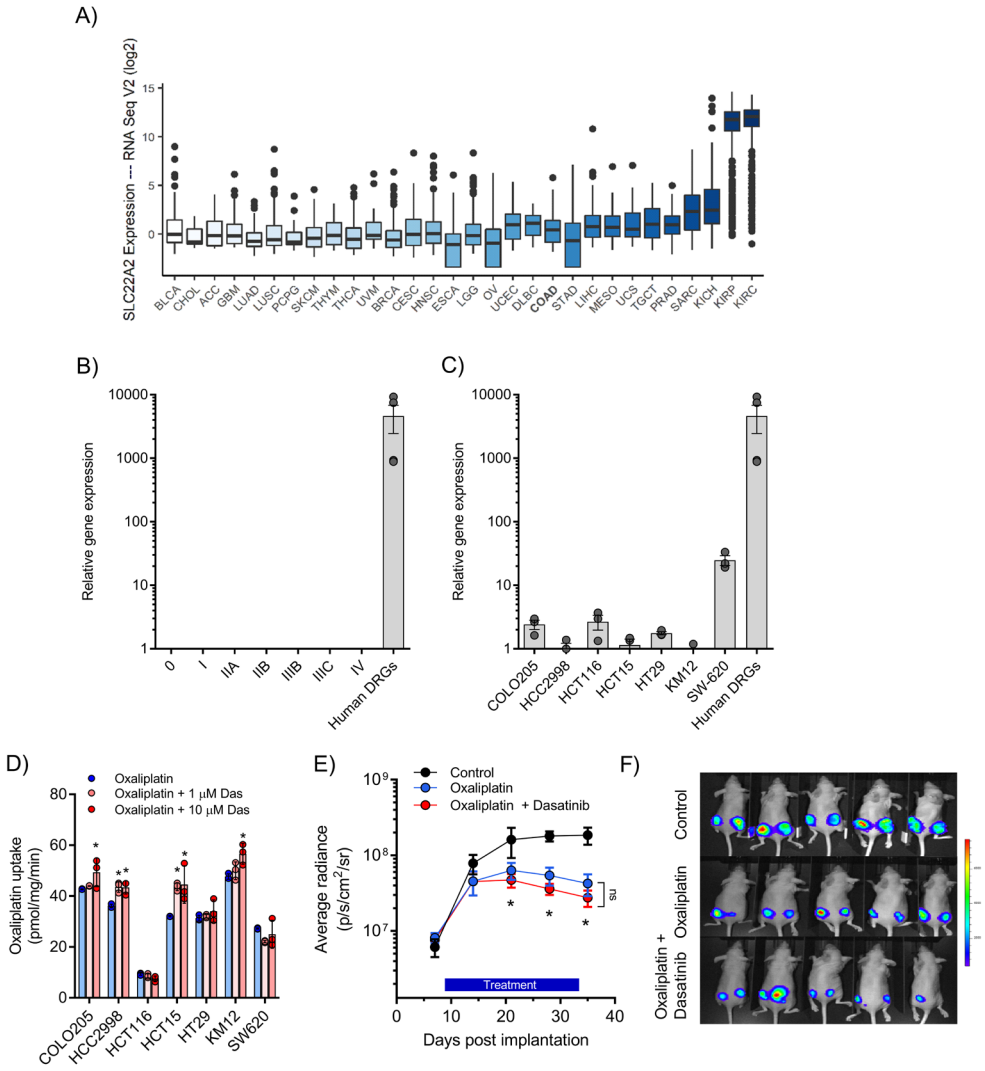

207

208 **Supplemental Figure 7. (A)** Log_2-transformed expression of OCT2 RNASeq data in human
209 cancers from the TCGA Pan-Cancer Analysis Project. The RNASeq data was imported into R,
210 using the CGDS package, organized by median gene expression and plotted using ggplot2. Low
211 throughput expression analysis of OCT2 using RT-qPCR from **(B)** Stage 0-IV primary human
212 colorectal tumor tissues (n=3) or **(C)** cancer cell lines (part of NCI-60) (n=3), compared to primary
213 resected human DRGs. **(D)** Accumulation of oxaliplatin in colorectal cancer cells under continuous
214 treatment with 1 or 10 μM dasatinib, as a surrogate marker of oxaliplatin uptake. **(E)** Average
215 radiance representing the bioluminescence imaging of HCT116-luciferase labeled tumors
216 implanted in male athymic nude mice (n=5-10) with **(F)** five representative luminescence images
217 of each group. Data presented represents the mean ± standard error of the mean (SEM). *P<0.05
218 compared to control tumor radiance at each individual imaged time.

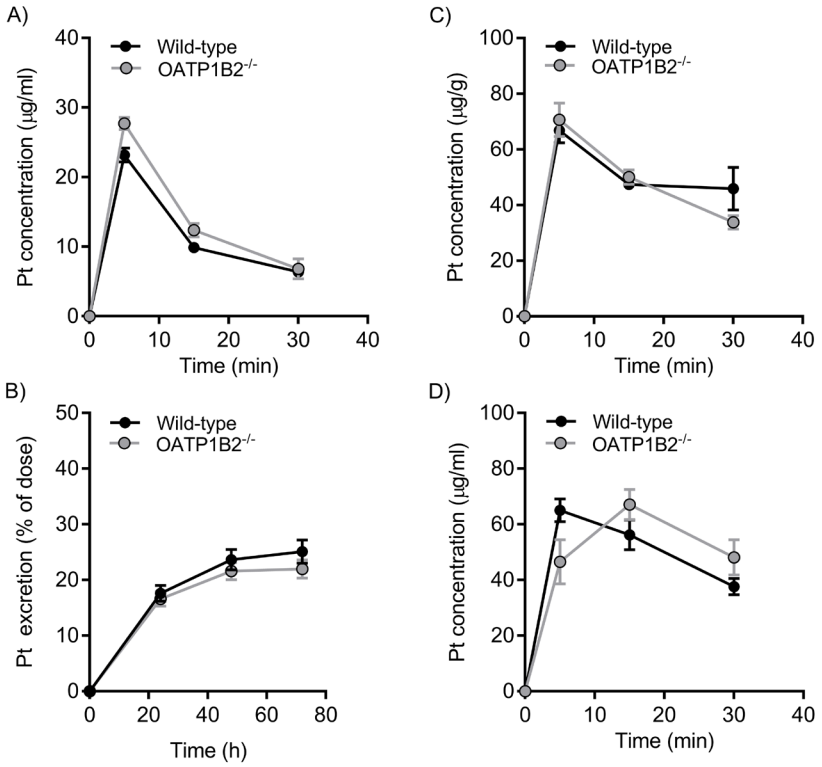

219

220 **Supplemental Figure 8.** Pharmacokinetics and distribution profile of oxaliplatin in **(A)** plasma,
221 **(B)** feces, **(C)** kidney and **(D)** liver from wild-type or OATP1B2-deficient mice (n=5) following
222 treatment with a single injection of 10 mg/kg oxaliplatin. Data presented represents the mean ±
223 standard error of the mean (SEM).

224

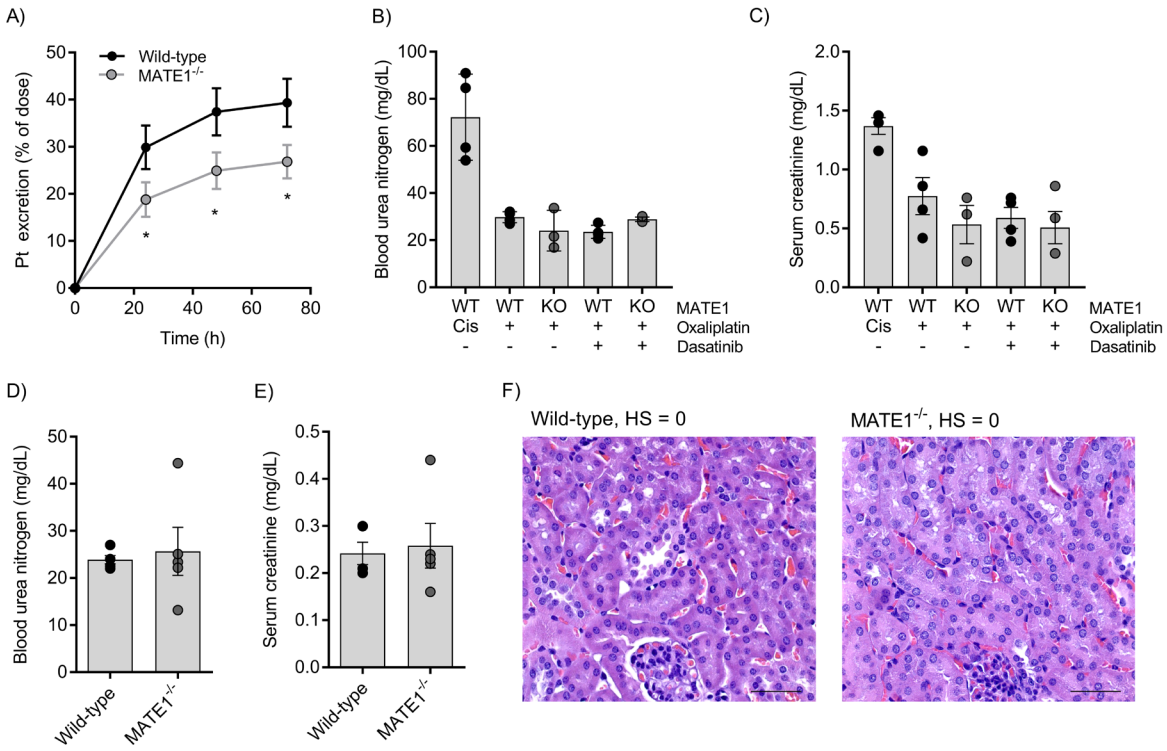

225

226 **Supplemental Figure 9**. **(A)** Urinary excretion of oxaliplatin in wild-type or MATE1-deficient mice,
227 expressed as a percentage of the total administered dose. Serum markers of impaired renal
228 function: **(B)** blood urea nitrogen (BUN) and **(C)** creatinine (sCr) in wild-type or MATE1-deficient
229 mice pre-treated with dasatinib 30 minutes prior to oxaliplatin. All animals in (A-C) received a
230 single injection of 10 mg/kg oxaliplatin and/or 15 mg/kg dasatinib. *P<0.05 compared to wild-type
231 at each individual time-point. Serum markers of impaired renal function: **(D)** BUN and **(E)** sCr and
232 **(F)** morphological evaluation in cross-sections of kidneys (magnification 40x) in wild-type or
233 MATE1-deficient mice treated with a single supra-dose of 40 mg/kg oxaliplatin. All data presented
234 represents the mean ± standard error of the mean (SEM).

235

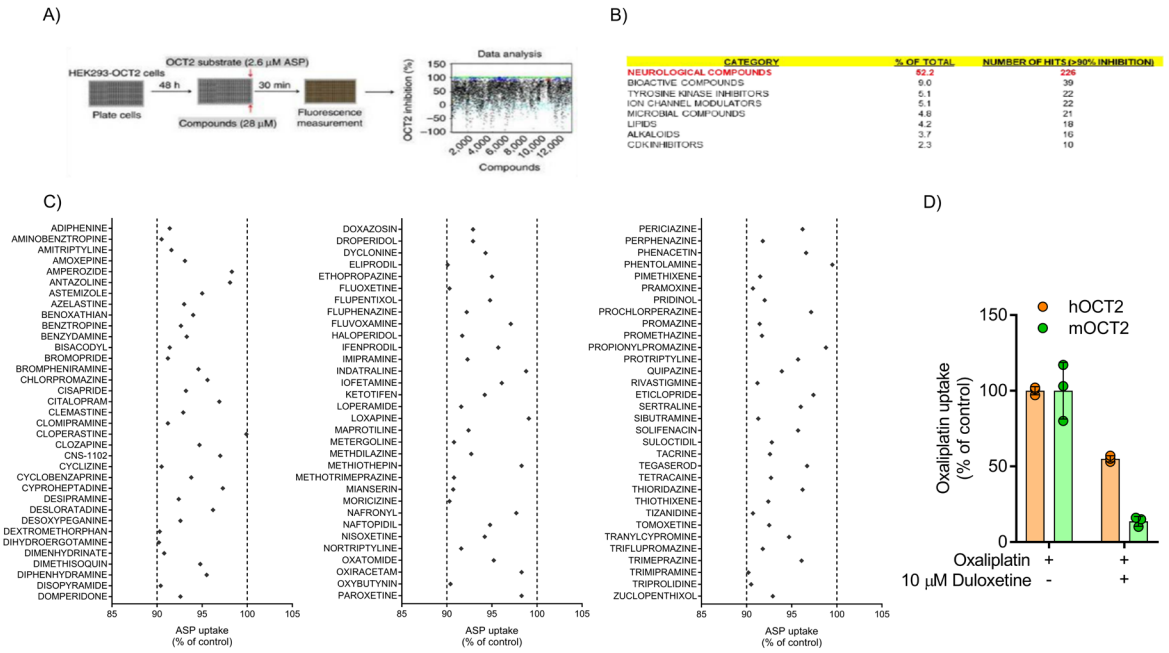

236

237 **Supplemental Figure 10. (A)** High-throughput workflow to identify OCT2 inhibitors (10) using
238 ASP as a prototypical transport substrate and fluorescence as a surrogate marker for OCT2
239 function. **(B)** Classification of compounds (433/8086) that inhibited OCT2 function by >90%. **(C)**
240 Putative list of neurological compounds that inhibit OCT2 (>90%). **(D)** Relative OCT2 function
241 (n=3) as measured by intracellular accumulation of oxaliplatin in mouse or human OCT2 and
242 inhibition by 10µM duloxetine. Data presented represents the mean ± standard error of the mean
243 (SEM); *P<0.05; compared to oxaliplatin conrtol.

244

Supplemental References

1. Chen M, Hu S, Li Y, Gibson AA, Fu Q, Baker SD, and Sparreboom A. Role of OATP2B1 in drug absorption and drug-drug interactions. *Drug Metab Dispos.* 2020.
2. Zwart R, Verhaagh S, Buitelaar M, Popp-Snijders C, and Barlow DP. Impaired activity of the extraneuronal monoamine transporter system known as uptake-2 in Orct3/Slc22a3-deficient mice. *Mol Cell Biol.* 2001;21(13):4188-96.
3. Kato Y, Kubo Y, Iwata D, Kato S, Sudo T, Sugiura T, Kagaya T, Wakayama T, Hirayama A, Sugimoto M, et al. Gene knockout and metabolome analysis of carnitine/organic cation transporter OCTN1. *Pharm Res.* 2010;27(5):832-40.
4. Li Q, Peng X, Yang H, Wang H, and Shu Y. Deficiency of multidrug and toxin extrusion 1 enhances renal accumulation of paraquat and deteriorates kidney injury in mice. *Mol Pharm.* 2011;8(6):2476-83.
5. Zaher H, Meyer zu Schwabedissen HE, Tirona RG, Cox ML, Obert LA, Agrawal N, Palandra J, Stock JL, Kim RB, and Ware JA. Targeted disruption of murine organic anion-transporting polypeptide 1b2 (Oatp1b2/Slco1b2) significantly alters disposition of prototypical drug substrates pravastatin and rifampin. *Mol Pharmacol.* 2008;74(2):320-9.
6. Marmiroli P, Riva B, Pozzi E, Ballarini E, Lim D, Chiorazzi A, Meregalli C, Distasi C, Renn CL, Semperboni S, et al. Susceptibility of different mouse strains to oxaliplatin peripheral neurotoxicity: Phenotypic and genotypic insights. *PLoS One.* 2017;12(10):e0186250.
7. Renn CL, Carozzi VA, Rhee P, Gallop D, Dorsey SG, and Cavaletti G. Multimodal assessment of painful peripheral neuropathy induced by chronic oxaliplatin-based chemotherapy in mice. *Mol Pain.* 2011;7(29.
8. Poulsen JN, Larsen F, Duroux M, and Gazerani P. Primary culture of trigeminal satellite glial cells: a cell-based platform to study morphology and function of peripheral glia. *Int J Physiol Pathophysiol Pharmacol.* 2014;6(1):1-12.
9. Leblanc AF, Huang KM, Uddin ME, Anderson JT, Chen M, and Hu S. Murine Pharmacokinetic Studies. *Bio Protoc.* 2018;8(20).
10. Sprowl JA, Ong SS, Gibson AA, Hu S, Du G, Lin W, Li L, Bharill S, Ness RA, Stecula A, et al. A phosphotyrosine switch regulates organic cation transporters. *Nat Commun.* 2016;7(10880.